On the structural dynamics of laminated composite plates and sandwich structures; a new perspective on damping identification

Fabien Marchetti, Kerem Ege, Quentin Leclere, N.B. Roozen

On the structural dynamics of laminated composite plates and sandwich structures; a new perspective on damping identification.

Fabien Marchetti *

Univ Lyon, INSA-Lyon, LVA EA677, F-69621 Villeurbanne, France

Kerem Ege

Univ Lyon, INSA-Lyon, LVA EA677, F-69621 Villeurbanne, France

Quentin Leclère

Univ Lyon, INSA-Lyon, LVA EA677, F-69621 Villeurbanne, France

N.B. Roozen

KU Leuven, Laboratory of Acoustics, Department of Physics and Astronomy, Celestijnenlaan 200D, B-3001 Heverlee, Belgium

---

Abstract

This paper presents the modelling and the dynamic characterization of laminated composite plates and sandwich structures in terms of stiffness and damping. The developments used in this paper are based on the analytical multilayer model of Guyader and Lesueur (JSV, 1978). The model considers linear shear, membrane and bending effects in each layer. The characteristics of the structure are determined by means of an equivalent thin plate methodology. The first main novelty of this paper consists in adapting this methodology for laminated plates (orthotropic multilayers with arbitrary orthotropic angle per layer). An experimental validation of this adaptation is presented for a laminated composite plate. Concerning the modelling of the structural loss factor, a space domain definition based on the spatial attenuation of a plane wave is compared to an energetic method and an equivalent definition based on the thin plate theory. The results show that the equivalent definition overestimates the loss factor in high frequencies since the thin plate theory only considers the flexural behaviour of the structure. On the contrary, the space domain definition (which give similar results as compared to the energetic one for lightly damped structures) considers the frequency dependent variation of the dynamic behaviour of the structure by means of the ratio between the group and phase velocities. The latter approach is considered to be more correct. The second main novelty of this article is on the experimental validation of this space domain definition. The structural loss factors of two sandwich structures are

Article published in Journal of Sound and Vibration

identified from measurements using modal, energetic and spatial methods. The results using the space domain definition are in very good agreement with the analytical predictions and the estimations of the modal and energetic methods for both plates for a large frequency band (up to 20 kHz), demonstrating the validity of the approach developed in this paper.

Key words: Sandwich panels; laminated composite structures; equivalent plate model; flexural rigidities; structural loss factor; space and time domain estimations; experimental validations

---

1 Introduction

Nowadays, complex materials are more and more used in transport and building industries to combine a reduced weight with an increased stiffness. Among these materials, multi-layered structures such as laminated composite plates stand out because of their high stiffness and low mass.

In the literature, several analytical models exist to handle such structures. Using these models, the structural parameters such as Young's modulus and loss factor of an equivalent anisotropic single layer plate can be identified as function of frequency. Carrera [1] separates these models in two main groups.

The first group, the Equivalent Single Layer (ESL) models, describes the multilayer material by means of an equivalent mono-layer that resembles the dynamic behaviour of the multilayer, for a given frequency, as good as possible. Obviously, the material properties of the equivalent mono-layer are dependent upon frequency. The model of Ross, Kerwin and Ungar [2], developed for a multilayer consisting of three layers, fits perfectly within this group. In this model, a simplified energetic approach is used with several assumptions (for example that the total dissipation of energy is described by the shear deformation of the core). Two other papers of Kerwin [3] and Ungar [4] follow the same approach. Ungar defines the loss factor for each wave type in terms of strain energy. Nilsson and Nilsson [5] studied honeycomb sandwich beams, taking into consideration bending, shear and rotation effects in each layer. The Hamilton's principle is applied to identify the different types of wave propagating inside the beam. Backström and Nilsson [6] estimate the equivalent loss factor of multilayered beams by identifying the bending wavenumber of the structure with the one of an Euler-Bernouilli beam. Recently Nilsson et al. [7]

* corresponding author
Email addresses: fabien.marchetti@matelys.com (Fabien Marchetti), kerem.ege@insa-lyon.fr (Kerem Ege), quentin.leclere@insa-lyon.fr (Quentin Leclère), bert.roozen@kuleuven.be (N.B. Roozen).

studied the influence of length and boundary conditions on the apparent bending stiffness of sandwich beams.

The second main group of Carrera is called Layer Wise (LW) models, where a displacement field is defined for each layer. For example, the model of Ghinet and Atalla [8], developed for laminated structures, considers a Reissner−Mindlin displacement field for each layer. Equilibrium equations lead to the dispersion relations of the plate. For the special case of a multilayer system consisting of three layers, of which the core layer is relatively thick and soft, Ghinet adds a dilatational motion along the core's thickness to include the symmetric mode. Finite element models were also developed such as the one of Shorter [9] for a multilayered structure with isotropic material properties. Shorter uses a one-dimensional mesh and an eigenvalue problem is set up to identify the dispersion curves. In Ghinet's and Shorter's papers, the loss factor is defined with the strain energy method. Manconi and Mace [10] present a three-dimensional wave finite element method for predicting dispersion and dissipation of waves in viscoelastic laminated panels. They describe several ways to define the loss factor: with the strain energy at a real prescribed frequency or with an averaging as function of the direction if the material is a laminated plate.

The model of Guyader and Lesueur [11] establishes also one kinematic for each layer and has a number of kinematic variables independent of the number of layer. These two aspects make such an analytical model faster than numerical (FEM) or other analytical (Layer Wise) models and more accurate than Equivalent Single Layer models. In another paper, Guyader and Cacciolati [12] used this model to characterise the multilayer assuming that the structure exhibits the same behaviour as a Love-Kirchhoff's thin plate. Contrarily to ESL models, which look for equivalent parameters that are constant in frequency, this equivalence is considered at each frequency leading to equivalent parameters that depend on frequency.

Different experimental procedures exist for the characterisation of multilayer structures. At high frequencies, where modal analysis approaches become unpractical because of the increased modal density [13], other techniques based on vibration field analysis have demonstrated their efficiency, as detailed by Ege et al. [14]. Among them, the IWC (Inhomogeneous Wave Correlation) method stands out, which is basically a wave fitting approach used by Berthaut [15] on ribbed panels and by Cherif et al. [16] on honeycomb sandwich structures. The ISM (Image Source Method), described by Cuenca et al. [17], estimates the vibration field of polygonal plates with Green's functions taking into account reflections on edges with image sources. Roozen et al. [18] used this technique to fit measurements of point-excited plate structures and identify material parameters. In a different way, the CFAT (Corrected Force Analysis Technique) methodology [19], recently extended for laminated structures [20], estimates the equations of motion of a plate with a finite difference scheme applied on the measurement field. Structural parameters are identified by measuring far from the source. Similarly, the VFM (Virtual

Field Method) [21,22], the pressure is estimated with virtual displacement and curvature fields. In another recent approach, Margerit et al. developed a promising characterisation method using ESPRIT algorithm to extract complex wavevector for 1D [23] and 2D [24] structures in wide frequency range.

This article deals with, on one part, the modelling of laminated plates, which can be described as multilayers with oriented orthotropic layers, and, on the other part, the modelling of structural damping. The manuscript is organized in 3 sections. In a first section, we propose an adaptation of the "equivalent thin plate" methodology of Guyader and Cacciolati [12], initially developed for isotropic materials, for laminated plates. An experimental validation of this adaptation, focused on the real part of the stiffness, is conducted on a composite laminated panel. In a second section, the modelling of the structural loss factor is discussed by means of a comparison of three definitions using the results of the bibliography [6,8,9]. The first approach is based on the spatial attenuation of a plane wave while the second one uses an equivalent model based on the thin plate theory and the third one corresponds to the Modal Strain Energy (MSE) method. In a third section, the structural loss factors of sandwich plates are experimentally estimated using the CFAT method with the space domain and equivalent definitions. The results are compared to the predictions of the analytical model of Guyader et al. [11,12] and to the experimental estimations of modal and energetic methods.

The principal novelties of this paper can be summarized as follows:

- Starting from the analytical model of Guyader and Lesueur [11] and Woodcock [25], the equations of motion are solved to obtain the dispersion relationship of the laminated structure using a symbolic computation.
- The equivalent methodology of Guyader and Cacciolati [12] is adapted for laminated structures by defining the equivalent thin plate with 5 flexural rigidities.
- The space domain definition of the structural loss factor is experimentally validated on sandwich plates by comparing the results with the ones of modal and energetic methods for a large frequency band (up to 20 kHz).

2 Model

2.1 Hypothesis

The developments in this paper are based on the analytical model of Guyader and Lesueur [11]. This simplified multilayer model describes the behaviour of each layer with a Reissner-Mindlin displacement field. In addition to the flexural (W) and membrane (ψ) motions, this kinematic considers a linear shear (ϕ) inside each

layer. Although less influential in the low frequency range, the effect of this shear can be significant on the prediction of the bending mode at higher frequencies. In addition, the transverse displacement is supposed to be constant for all layers, neglecting the deformation through the thickness. Continuity conditions between layers lead to equations of motion which are independent of the number of layers. In this way, the behaviour of the whole multilayer is defined by the kinematic variables of one reference layer. An energetic aspect governed by Hamilton's principle is used to derive the equations of motion of the multilayer. A specific solution of this equation leads to the dispersion curves of the plate.

2.2 Comparison with a finite element model

In order to illustrate the performances of the model, we compared its results in terms of dispersion curves with the Spectral Finite Element Method (SFEM) used by Shorter [9]. This comparison concerns the modelling of a sandwich panel composed of three isotropic layers and is presented in Figure 1. The characteristics of this sandwich are mentioned in Table 1.

	h (mm)	ρ (kg.m^{-3})	E (GPa)	ν (-)
Skins	0.6	2700	71	0.33
Core	15	48	0.03	0.2

Table 1
Characteristics of a sandwich panel simulated by Shorter with the SFEM.

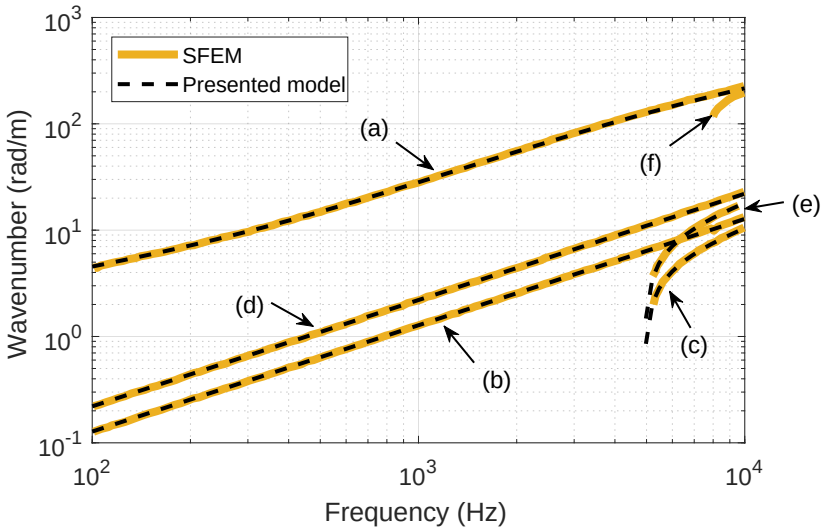

Fig. 1. Dispersion curves of the propagating modes of an isotropic sandwich panel predicted by the SFEM [9] (yellow solid curves) and the model of Guyader and Lesueur (black dashed curves).

The five dispersion curves identified by the analytical model are similar to the re-

sults of the SFEM. They correspond to five propagating waves: flexural (a), membrane (b) and shear (c) in the longitudinal direction as well as membrane (d) and shear (e) in the transverse direction. As mentioned in section 2.1, the model of Guyader and Lesueur assumes a constant transverse displacement in each layer, neglecting the deformation through the thickness. Because of this, curve (f), corresponding to a symmetric wave propagating along the thickness of the multilayer (the S0 mode of Lamb wave theory [26]), is not found by this model. In the case of a three layers sandwich, Ghinet and Atalla [8] add a dilatational motion to the core to describe this symmetric mode. This addition involves to use a Rayleigh-Ritz method with hierarchical trigonometric form functions and implies a huge amount of calculation time in comparison to the model presented in this paper.

2.3 Dispersion curves for laminated structures

Guyader and Lesueur [11] consider in their model orthotropic layers whose orthotropic axes are aligned with the main axes of the plate ($\theta_n = 0°, 90°$). Their formulation has been extended by Woodcock [25] for laminated plates ($\theta_n \neq 0°, 90°$) up to the Hamilton's principle (Eq. (1)). Then, the first novelty of this paper is to establish, from the work of Woodcock, the equations of motion and the analytical writing of the stiffness and mass matrices of this type of structure. The second novelty concerning our model consists in giving the expression of the dispersion relation using symbolic computation.

The Hamilton's principle defines the action of the system during a time interval $[t_0; t_1]$ over a functional H integrated on the surface of the plate $a \times b$:

$$H = \int_{t_0}^{t_1} \int_{-a/2}^{a/2} \int_{-b/2}^{b/2} (e_\mathrm{k} - e_\mathrm{d}) \mathrm{d}x \mathrm{d}y \mathrm{d}t, \tag{1}$$

where both, e_k the kinetic energy and e_d the deformation energy, are given by Woodcock [25]. These energies respectively depend on 18 coefficients δ_i and 69 coefficients λ_i defined by the characteristics of the layers (see the appendices B.3 and B.4 of Loredo and Castel [27]). Thanks to the coupling relations of the model, the Hamilton's functional only depends on the five kinematic variables of the first layer, described by the vector:

$$\{\mathcal{W}\} = \left\{ W,\, \psi_x^1,\, \varphi_x^1,\, \psi_y^1,\, \varphi_y^1 \right\}^\mathrm{T}. \tag{2}$$

A minimization of the action of Hamilton's functional by using the differential form of Euler-Lagrange for each variables of $\{\mathcal{W}\}$ leads to a matrix expression of the

equations of motion described by:

$$\left([I]\frac{\partial^2}{\partial t^2}+[J]\right)\{\mathcal{W}\}=\{0\}, \tag{3}$$

where $[I]$ (respectively $[J]$), defined in the appendix, contains all the coefficients δ_i (respectively λ_i) expressed in the equation of e_{k} (respectively e_{d}).

As proposed by Guyader and Cacciolati [12] or by Ghinet and Atalla [8], the equation of motion can be solved using a plane wave propagating in a direction with an angle θ relative to the reference coordinate system and described by a harmonic motion with angular frequency ω and a wave number $k(\theta,\omega)$:

$$\{\mathcal{W}\}=\{\overline{\mathcal{W}}\}\mathrm{e}^{-\mathrm{j}k[x\cos(\theta)+y\sin(\theta)]}\mathrm{e}^{\mathrm{j}\omega t}, \tag{4}$$

where $\{\overline{\mathcal{W}}\}$ corresponds to the complex amplitude of $\{\mathcal{W}\}$.

This specific solution (4), inserted into the equation of motion (3), leads to the system:

$$\left([\mathcal{K}]-\omega^2[\mathcal{M}]\right)\{\overline{\mathcal{W}}\}=\{0\}, \tag{5}$$

with $[\mathcal{K}]$ the stiffness matrix associated to the deformation energy:

$$[\mathcal{K}]=\begin{bmatrix} k^4l_1 & \mathrm{j}k^3l_2 & \mathrm{j}k^3l_3 & \mathrm{j}k^3l_4 & \mathrm{j}k^3l_5 \\ -\mathrm{j}k^3l_2 & k^2l_6 & k^2l_7 & k^2l_8 & k^2l_9 \\ -\mathrm{j}k^3l_3 & k^2l_7 & k^2l_{10}+l_{37} & k^2l_{11} & k^2l_{12}+l_{69} \\ -\mathrm{j}k^3l_4 & k^2l_8 & k^2l_{11} & k^2l_{13} & k^2l_{14} \\ -\mathrm{j}k^3l_5 & k^2l_9 & k^2l_{12}+l_{69} & k^2l_{14} & k^2l_{15}+l_{38} \end{bmatrix}, \tag{6}$$

and $[\mathcal{M}]$ the mass matrix associated to the kinetic energy:

$$[\mathcal{M}]=\begin{bmatrix} k^2d_1+d_8 & \mathrm{j}kd_2 & \mathrm{j}kd_3 & \mathrm{j}kd_4 & \mathrm{j}kd_5 \\ -\mathrm{j}kd_2 & d_6 & d_7 & 0 & d_9 \\ -\mathrm{j}kd_3 & d_7 & d_{10} & d_{11} & d_{12} \\ -\mathrm{j}kd_4 & 0 & d_{11} & d_{13} & d_{14} \\ -\mathrm{j}kd_5 & d_9 & d_{12} & d_{14} & d_{15} \end{bmatrix}. \tag{7}$$

The coefficients l_i and d_i are given in the appendix.

Non trivial solutions of Eq. 5 are obtained for:

$$\det\Big([\mathcal{K}] - \omega^2[\mathcal{M}]\Big) = 0. \tag{8}$$

This determinant is solved using the symbolic toolbox of the software program Matlab from The MathWorks, Inc., Massachusetts, USA. The results of this symbolic computation are available as a supplementary material of the paper in the form of a Matlab script. The determinant corresponds to a 6th order polynomial in k^2 meaning that the model can identify the dispersion curves of up to six different wave types if we consider positive values of k only. Five of them have been illustrated on the example presented in section 2.2. The sixth root correspond to an evanescent wave which is not studied in this paper since we are interested in propagating waves.

2.4 Equivalent thin plate

As stated in the introduction, Guyader and Cacciolati [12] use an equivalent plate to characterize the multilayer. This method determines, for a given frequency, the complex flexural rigidity D of an equivalent single layer plate under Love-Kirchhoff thin plate theory, in order to exhibit the same transverse displacement as the multilayer.

This equivalent methodology was initially set up for isotropic materials. Then, we propose, as the third novelty of this paper, to adapt it for laminated panels. The equation of motion of such a structure under Love-Kirchhoff's theory is defined by five flexural rigidities D_{ij}:

$$D_{11}\frac{\partial^4 W}{\partial x^4} + D_{22}\frac{\partial^4 W}{\partial y^4} + D_{12}\frac{\partial^4 W}{\partial x^2 \partial y^2} + D_{16}\frac{\partial^4 W}{\partial x^3 \partial y} + D_{26}\frac{\partial^4 W}{\partial x \partial y^3} = -\rho h \frac{\partial^2 W}{\partial t^2}, \tag{9}$$

where h is the total thickness of the multilayer and ρ represents the density of the multilayer and is estimated by the equation:

$$\rho = \frac{\sum_n h_n \rho_n}{\sum_n h_n}. \tag{10}$$

A specific solution of the Eq. (9), similar to the one of the multilayer (4), describes the flexural propagating wave inside the plate with a wavenumber $k_{\mathrm{f}}(\theta, \omega)$:

$$W = w\mathrm{e}^{-\mathrm{j}k_{\mathrm{f}}[x\cos(\theta)+y\sin(\theta)]}\mathrm{e}^{\mathrm{j}\omega t}, \tag{11}$$

and leads to the dispersion relation:

$$k_{\mathrm{f}}^4 \left(D_{11}c^4 + D_{22}s^4 + D_{12}c^2s^2 + D_{16}c^3s + D_{26}cs^3 \right) = \rho h \omega^2, \tag{12}$$

with $c = \cos(\theta)$ and $s = \sin(\theta)$.

The equivalent methodology assumes that k_{f} is equal to the flexural wavenumber obtained as a root of Eq. (8). The equivalent parameters D_{ij} can be identified by applying Eq. (12) for i values (at least 5) of the angle θ equally spaced in the interval $[0, \pi[$. Angles larger than $180°$ were not considered since the dispersion relation (12) is π periodic. Then, for a given angular frequency ω, the following matrix relation can be written:

$$\Big[\Delta\Big]\Big\{\beta\Big\} = \rho h \omega^2 \Big\{\kappa\Big\}, \tag{13}$$

with

$$\Big[\Delta\Big] = \begin{bmatrix} c_1^4 & s_1^4 & c_1^2 s_1^2 & c_1^3 s_1 & c_1 s_1^3 \\ \vdots & \vdots & \vdots & \vdots & \vdots \\ c_i^4 & s_i^4 & c_i^2 s_i^2 & c_i^3 s_i & c_i s_i^3 \end{bmatrix}; \quad \begin{aligned} c_1 &= \cos(\theta_1); \\ s_1 &= \sin(\theta_1); \\ c_i &= \cos(\theta_i); \\ s_i &= \sin(\theta_i); \end{aligned}$$

$$\Big\{\kappa\Big\} = \begin{pmatrix} \dfrac{1}{k_{\mathrm{f}}^4(\omega, \theta_1)} \\ \vdots \\ \dfrac{1}{k_{\mathrm{f}}^4(\omega, \theta_i)} \end{pmatrix}; \quad \Big\{\beta\Big\} = \begin{pmatrix} D_{11}(\omega) \\ D_{22}(\omega) \\ D_{12}(\omega) \\ D_{16}(\omega) \\ D_{26}(\omega) \end{pmatrix}.$$

The flexural rigidities D_{ij} are identified by means of a generalized inverse approach:

$$\Big\{\beta\Big\} = \rho h \omega^2 \left(\Big[\Delta\Big]^{\mathrm{T}} \Big[\Delta\Big] \right)^{-1} \Big[\Delta\Big]^{\mathrm{T}} \Big\{\kappa\Big\}. \tag{14}$$

By doing this approach for all frequencies, the 5 dynamic bending stiffness of the equivalent plate can be obtained as function of frequency.

2.5 Experimental estimation of the equivalent rigidities of a laminated composite plate

This section concerns the experimental validation of the equivalent methodology for laminated plates.

A carbon fiber composite plate, supplied by the company Hexcel (Dagneux, France) is studied. The plate is composed of four layers with different orientations of the fibers (60°/-60°/-60°/60°). This symmetric pile reveals that the plate is monoclinic and is defined by 5 rigidities under Love-Kirchhoff's theory. The dimensions of the plates are 0.6×0.8 m^2 with a total thickness of 0.748 mm and a density of 1540 kg.m^{-3}. The structure is excited by a shaker, using white noise from 1 to 10 kHz and its displacement field is measured by means of a scanning Laser Doppler Vibrometer (Polytec, PSV-400) across the red area as indicated in Figure 2. A measurement mesh of 55×57 points is used. The spacing between consecutive points of the mesh in the x and y direction is $\Delta_x = \Delta_y = 5.3$ mm.

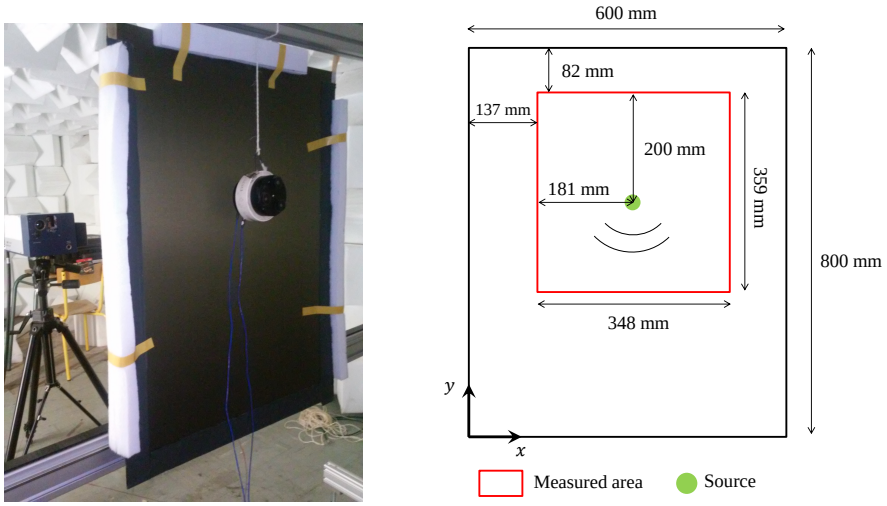

Fig. 2. Experimental setup.

The wave fitting approach IWC [15,16,28] (Inhomogeneous Wave Correlation) is used for the processing of the measured data. A correlation function, given by Eq. (15), between the measured displacement field w and a plane wave Eq. (16) is calculated, for a given angular frequency ω, as function of the propagating parameters (k, θ).

$$\mathrm{IWC}(k,\theta) = \frac{|\sum_m \sum_n \mathcal{C}_{m,n} w_{m,n} \sigma^*_{m,n}(k,\theta)|}{\sqrt{\sum_m \sum_n \mathcal{C}_{m,n} |w_{m,n}|^2 \sum_m \sum_n \mathcal{C}_{m,n} |\sigma_{m,n}(k,\theta)|^2}}, \tag{15}$$

with:

$$\sigma_{m,n}(k,\theta) = \mathrm{e}^{-\mathrm{j}k(x_m \cos(\theta) + y_n \sin(\theta))}, \tag{16}$$

where superscript * denotes the complex conjugate, x_m, y_n correspond to the position of a point on the rectangular mesh, and $\mathcal{C}$ to the coherence between the input signal and the measured vibration velocity field. The value of k that maximizes the correlation function Eq. (15) is considered as the flexural wavenumber of the plate. Then, the IWC method is run for each angular frequency ω and at different values of propagating angle θ to identify the flexural wavenumber $k_\mathrm{f}(\theta, \omega)$ as function of these two parameters. The flexural rigidities of the plate are experimentally determined as function of frequency by applying the equivalent methodology described

in section 2.4 from the measured flexural wavenumber $k_{\mathrm{f}}(\theta, \omega)$.

As the virtual field (Eq. (16)) used in this fitting approach doesn't consider the reflected waves, foam was added to the edges of the plate (see Figure 2) to attenuate theses reflections in order to increase the correlation factor (Eq. (15)).

In order to validate the extension of the equivalent methodology presented in section 2.4, the multilayer has been simulated with the model. Several simulations has been done for different values of the material parameters (only the Young moduli E_x, E_y and the shear modulus G_{xy}) of the layers. Then, we selected the optimal parameters that minimize the differences between the predicted rigidities of the model and the ones estimated by IWC on the whole frequency band. These optimal parameters are very closed to the ones of the manufacturer (see Table 2). The comparison of the experimental and analytical rigidities are presented in Figure 3. In theory, the flexural rigidities depend on frequency according to the shearing of the structure. As the studied composite plate is thin, the shearing effect and the variations of the rigidities are minor in this frequency range. Oscillations observed in the low frequency range for experimental estimations are due to finite aperture effects of the Fourier analysis (related to the wavenumber resolution). The difficulty of estimating the D_{16} coefficient, as compared to the others, may be due to the least squares approach, that samples the curve $k_n(\theta)$ with a regular step in θ. Considering the shape of this curve, this might not be an optimal choice. For instance a regular sampling in terms of arc length of the $k_n(\theta)$ curve could have been an alternative, better approach.

	h	ρ	E_x	E_y	G_{xy}	ν_{xy}
Parameters supplied by the manufacturer	0.187 mm	1540 kg.m^3	145 GPa	9.6 GPa	4.6 GPa	0.31
Optimal parameters	0.187 mm	1540 kg.m^3	133 GPa	8.8 GPa	6.6 GPa	0.31

Table 2
Material parameters of one layer of the composite plate. Data supplied by the manufacturer and optimal parameters in order to minimize the difference between the prediction of the model and the results of IWC.

We can also noticed, on the K-space representation of the flexural wavenumber, the coupling effect between the flexural and torsional behaviour created by the specific orientations of the layers of this plate (see Figure 4).

3 Analytical estimation of the structural loss factor

The estimation of the structural loss factor of multilayered structures can be performed in various manners. In this section, three different approaches are pre-

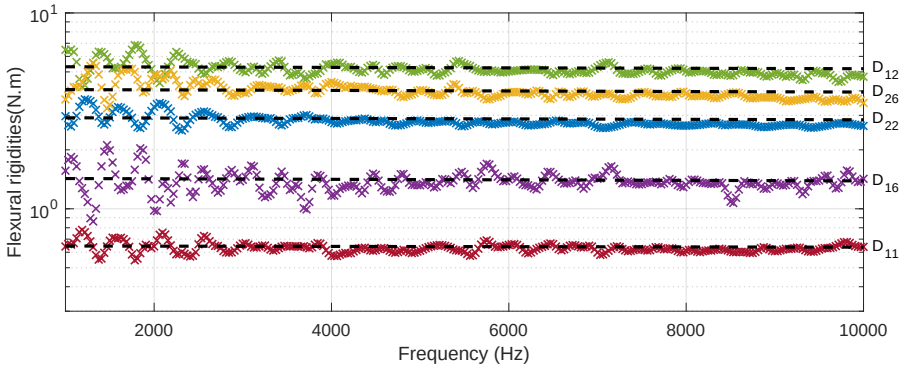

Fig. 3. Comparison of the bending stiffness (D_{11}: red, D_{22}: blue, D_{12}: green, D_{16}: magenta, D_{26}: yellow) of the composite plate estimated by IWC (cross) and predicted by the model (black dashed lines) with the optimal parameters (see Table 2).

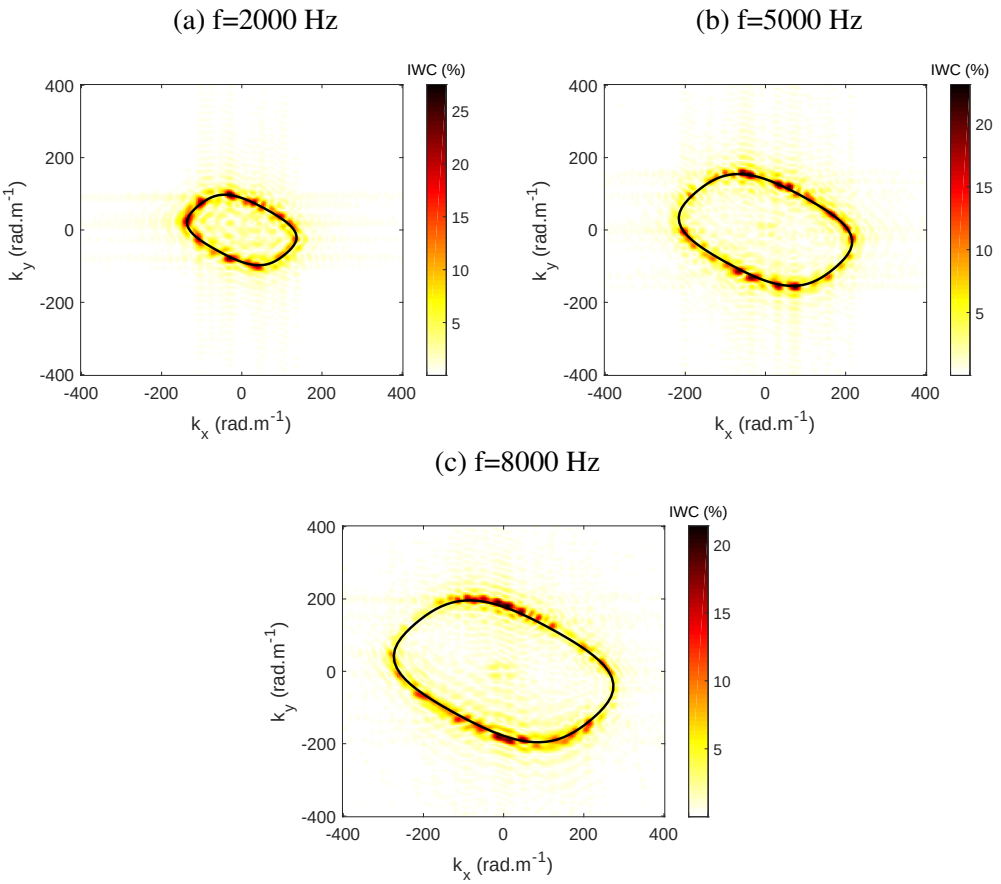

Fig. 4. K-space representation of the correlation factor of IWC applied on the measurements of the laminated composite plate at $f = 2$ kHz (a), 5 kHz (b) and 8 kHz (c). Flexural waveumber predicted by the model (black line).

sented: the first one exploits the space domain definition of the attenuation of a plane wave, while the second one is based on an equivalent model defined by the Love-Kirchhoff thin plate theory and the third one uses an energetic definition. The results obtained by these three approaches can be rather different, and are compared

with various numerical models from literature [6,8,9].

3.1 Space domain definition

The attenuation of a plane wave is naturally defined by a complex wavenumber, whose imaginary part defines the spatial decay rate of the wave (using the $\mathrm{e}^{\mathrm{j}\omega t}$ convention, see Eq. (4)):

$$\Delta x = 20\log\left(\mathrm{e}^{\mathrm{Im}(k)}\right) = 20\mathrm{Im}(k)/\ln(10) \text{ in dB/m}. \tag{17}$$

This definition is not directly related to the structural loss factor η, that governs the decay rate in the time domain:

$$\Delta t = 20\log\left(\mathrm{e}^{-\mathrm{Im}(\omega)}\right) = 20\log\left(\mathrm{e}^{-\eta\mathrm{Re}(\omega)/2}\right) = -10\eta\mathrm{Re}(\omega)/\ln(10) \text{ in dB/s}. \tag{18}$$

A link between space and time domain attenuations can however be established by introducing the group velocity of the wave (that represents the velocity at which the energy is conveyed), defined by $C_\mathrm{g} = \partial\omega/\partial k$. The group velocity gives a relationship between space and time attenuations: $\Delta t = \Delta x C_\mathrm{g}$, which brings:

$$\eta = -2\frac{\mathrm{Im}(k)}{\mathrm{Re}(\omega)}C_\mathrm{g} = -2\frac{\mathrm{Im}(k)}{\mathrm{Re}(k)}\frac{C_\mathrm{g}}{C_\phi}, \tag{19}$$

where $C_\phi = \mathrm{Re}(\omega)/\mathrm{Re}(k)$ is the phase velocity of the plane wave. This definition of the structural loss factor, firstly given by Lyon and Dejong [29], and then used by Berthaut [30] and Rak et al. [31], is valid for all type of structures and is not based on any kind of equivalent model assumptions.

3.2 Equivalent definition

The structural loss factor can also be defined using an equivalent model. In this section, we focus on the methodology described in section 2.4. The equivalent plate is described by the Love-Kirchhoff's theory governed by the dispersion relation (Eq. 12). From this dispersion relation, it follows that the loss factor can be described as function of the bending wavenumber k_f [14,16,31,32] (using the $\mathrm{e}^{\mathrm{j}\omega t}$ convention, see Eq. (11)):

$$\eta_\mathrm{eq} = -\frac{\mathrm{Im}(k_\mathrm{f}^4)}{\mathrm{Re}(k_\mathrm{f}^4)}. \tag{20}$$

This equivalent definition is based on the thin plate theory and is thus valid for thin structures only. The theory assumes a constant ratio $C_{\mathrm{g}}/C_{\phi} = 2$ and the definition of Lyon and DeJong (Eq. (19)) can be related to the equivalent loss factor (Eq. (20)) by the relation $\eta = \eta_{\mathrm{eq}} = -4\frac{\mathrm{Im}(k_{\mathrm{f}})}{\mathrm{Re}(k_{\mathrm{f}})}$ for lightly damped structures.

In general case, when the structure is complex, the dynamic behaviour is highly modified with the frequency band considered. For example, for a sandwich plate, the ratio C_{g}/C_{ϕ} varies with frequency between values equal to 1 (pure shearing motion) and 2 (pure bending motion). Figure 5 presents this ratio and the loss factors calculated (using the present model) from Eq. (20) and Eq. (19) for a sandwich plate having the characteristics as given in Table 3 with different value of the thickness of the core. For a thin core, the ratio is approximately equal to 2 for the whole frequency band as the behaviour of the multilayer is dominated by the bending motion (coherent with a dispersion relationship $k^4 = f(\omega^2)$). Thus, the two definitions of the loss factor are close. On the contrary for a thick core, the ratio tends to 1 when the loss factor reaches his maximum. In this frequency domain, the behaviour of the multilayer is dominated by the shearing of the core (coherent with a dispersion relationship $k^2 = f(\omega^2)$) and the equivalent loss factor is overestimated compared to the one given by Eq. (19).

3.3 Energetic definition

The energetic approach described in this paper corresponds to the modal strain energy (MSE) method. In this methodology, the dissipated power of the structure for the *i*th propagating wave with a wavenumber k_i is detailed by [29]:

$$P_{\mathrm{diss}} = 2\mathrm{Re}\left(-\mathrm{j}\omega\{\mathcal{W}_i\}^{\mathrm{H}}\left([\mathcal{K}_i] - \omega^2[\mathcal{M}_i]\right)\{\mathcal{W}_i\}\right), \tag{21}$$

where $[\mathcal{K}_i]$ and $[\mathcal{M}_i]$ respectively correspond to the stiffness and mass matrices related to the ith propagating wave and are calculated from $[\mathcal{K}]$ (Eq. 6) and $[\mathcal{M}]$ (Eq. 7) with $k = \mathrm{Re}(k_i)$.

The vector $\{\mathcal{W}_i\}$ corresponds to the amplitude of the displacement of the first layer and is the solution of the following equation, which can be solved with an eigenvalue problem:

$$\left([\mathcal{K}_i] - \omega^2[\mathcal{M}_i]\right)\{\mathcal{W}_i\} = \{0\}. \tag{22}$$

The structural loss factor is related to the dissipated power and the elastic energy $\mathcal{E}$ of the system:

$$\eta = \frac{P_{\mathrm{diss}}}{2\omega\mathcal{E}} = \frac{\mathrm{Im}\left(\{\mathcal{W}_i\}^{\mathrm{H}}\left([\mathcal{K}_i] - \omega^2[\mathcal{M}_i]\right)\{\mathcal{W}_i\}\right)}{\mathrm{Re}\left(\{\mathcal{W}_i\}^{\mathrm{H}}[\mathcal{K}_i]\{\mathcal{W}_i\}\right)}, \tag{23}$$

(a) Thickness of the core: 0.1 mm

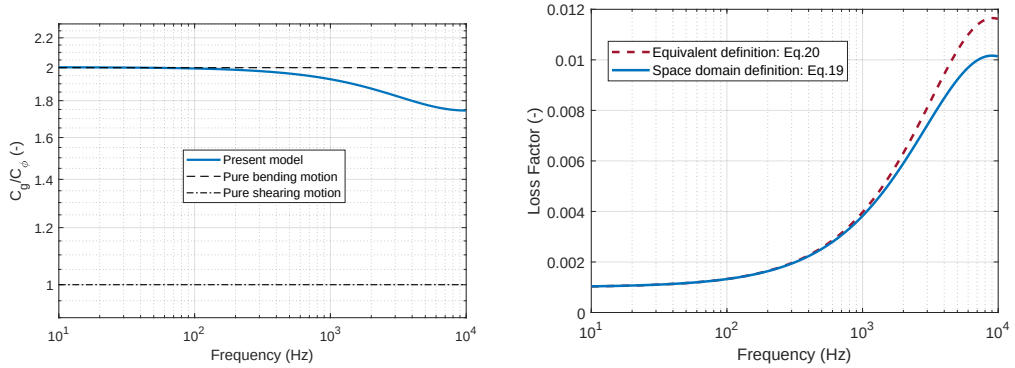

(b) Thickness of the core: 100 mm

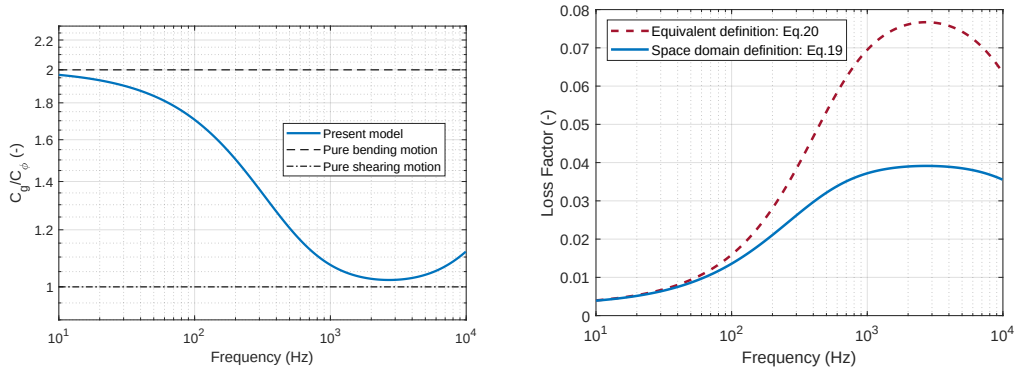

Fig. 5. Velocity ratios and comparisons of the equivalent and apparent loss factors of a sandwich plate with characteristics indicated in Table 3 for different value of the thickness of the core. Left: ratio $\frac{C_g}{C_\phi}$, right: loss factor. See the legend of the figures for the line types in the graphs.

with:

$$\mathcal{E} = \mathrm{Re}\left(\{\mathcal{W}_i\}^{\mathrm{H}}[\mathcal{K}_i]\{\mathcal{W}_i\}\right). \tag{24}$$

Manconi [10] uses the same energetic definition of the loss factor without taking into account the complex part of the mass matrix in the dissipated power. Shorter [9] and Ghinet [8] assume that the damping of each layer is uniform and the total dissipated power is a weighted sum of the dissipated power of each layer as detailed by:

$$\eta = \frac{\sum_{n=1}^{N} \eta_n \{\mathcal{W}_i\}^{\mathrm{H}}[\mathcal{K}_i^n]\{\mathcal{W}_i\}}{\{\mathcal{W}_i\}^{\mathrm{H}}[\mathcal{K}_i]\{\mathcal{W}_i\}}, \tag{25}$$

where $[\mathcal{K}_i^n]$ corresponds to the stiffness matrix of layer n related to the ith propagating wave and is calculated from $[\mathcal{K}_i]$ by considering only layer n. Contrarily to Eq. (23), the matrices of Eq. (25) are calculated with undamped material parameters since the damping of each layer is defined by η_n. In the case of composite laminated structures, where the damping of Young and shear modulus are not nec-

essary related, this assumption is not adapted.

3.4 Comparison with Backström: case of a multilayered beam

In this section a comparison of the results of our model with the results from Backström and Nilsson [6] is given, using the three definitions of the structural loss factor given in the previous sections.

Backström and Nilsson present an analytical model of asymmetric sandwich beams. The multilayered beam is compared to an Euler-Bernouilli beam and two different definitions of the loss factor are established from this comparison. The first one uses time-harmonic initial conditions, where the dissipation depends on space and the frequency is specified and real. In this case, the flexural wavenumber is complex and the definition of the equivalent loss factor is identical as the one presented previously with Love-Kirchhoff plate theory (Eq.50 of [6])(see Figure 7a). On the contrary, the second approach uses space-harmonic initial conditions, where the dissipation depends on time and the wavenumber is specified and real. No equivalent structure assumption is done here, and the damping is directly obtained solving the general equation of motion for linear vibrations $([\mathcal{K}] - \omega^2[\mathcal{M}])\{W\} = 0$ for a complex angular frequency (for further details reader can refer to [33]). Hence, the loss factor is simply defined as $\eta = \frac{\mathrm{Im}(\omega^2)}{\mathrm{Re}(\omega^2)}$ (Eq.21 of [6])(see Figure 7b).

	h (mm)	ρ (kg.m^{-3})	E (GPa)	G (GPa)	η (-)
First skin	0.75	2700	70	–	0.001
Core	10.2	74	0.130	0.045	0.04
Second skin	2	2700	70	–	0.001

Table 3
Characteristics of the sandwich beam of Backström [6].

Backström illustrates the comparisons between these two definitions of the loss factor for an aluminium/polymer/aluminium beam whose parameters are given in Table 3. This three layer plate has been simulated using the present model as well. Comparisons between our plate model and the finite beam model of Backstrom has been realised in terms of equivalent flexural rigidities (see Figure 6) and loss factors (see Figure 7). A classical value of 0.3 for Poisson ratios of the layers have been used in the present plate model.

The differences between Backström's results for the rigidity and the estimations of the present model (see Figure 6) can arise from the fact that the present model identifies the flexural rigidity of an equivalent plate and Backström's model, the one of an equivalent beam. Several factors can affect the results such as the Poisson ratio of the equivalent plate or the length of the equivalent beam.

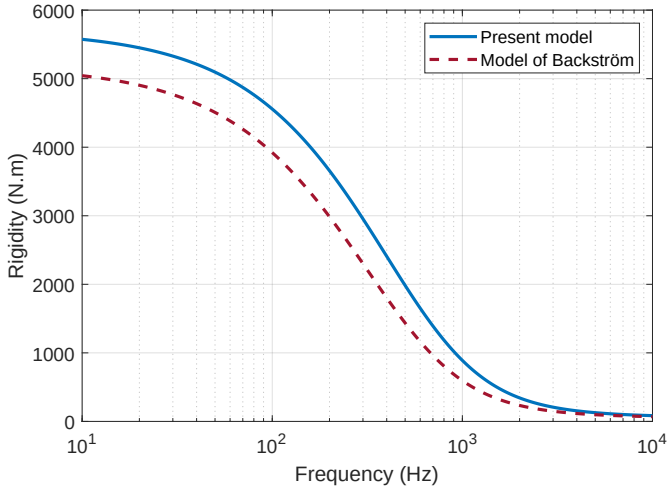

Fig. 6. Comparison of the flexural rigidities estimated by Backström's equivalent beam theory and the present equivalent plate model for the sandwich with material characteristics given in Table 3. Solid blue curve: present model, red dashed curve: model of Backström

(a) η_{eq} (b) η

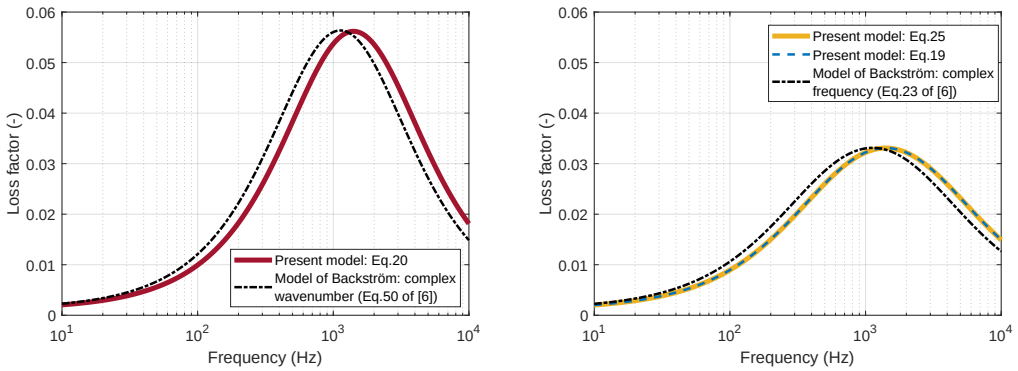

Fig. 7. Comparison of η_{eq} (a) and η (b) estimated by Backström's equivalent beam theory and the present equivalent plate model for the sandwich with material characteristics given in Table 3. The axes are the same for the two graphs. See the legend of the figures for the line types in the graphs.

The frequency evolution of the loss factors estimated by the present model (see Figure 7) are coherent with Backström's results. Such frequency dependence of the loss factor of sandwich structures has already been studied by Millithaler et al. [34] or Ege et al. [14,35] for a viscoelastic core, and by Butaud et al. [36] for a *Shape Memory Polymer* core. Whatever the method used, the loss factors reach a maximum at a certain frequency, depending on the structural dynamic parameters of the layers. At the frequency of maximum equivalent damping, the deformation is dominated by shear in the core. The amount of damping of the skins determines the damping of the structure at low and high frequencies. The stiffness of the layers determine the frequency at which a maximum in the loss factor occurs. This

frequency shifts as shown in Figure 7 are again caused by the differences in the stiffness between the two models.

We can see in Figure 7 that the space domain (Eq. (19)), the energetic (Eq. (25)) and the time domain ($\eta = \frac{\mathrm{Im}(\omega^2)}{\mathrm{Re}(\omega^2)}$) definitions give very similar results for this lightly damped structure. Both models are also in good agreements using the equivalent definition (Eq. (20)). As stated in section 3.2, this equivalent definition overestimates the loss factor since the flexural behaviour of the structure is dominated by the shearing of the core in the studied frequency band.

3.5 Comparison with Shorter: case of an isotropic multilayered plate

In a second validation of our model to determine the structural loss factor, results are compared with the work of Shorter [9]. Shorter applied the energetic definition of the loss factor (Eq. (25)) with the SFEM on an automotive glass laminate composed of sheets of glass separated with a layer of polyvinyl butyral (PVB). The PVB has a frequency dependent shear modulus and loss factor, detailed in [9]. The other parameters of the sandwich are mentioned in Table 4. Shorter has estimated the loss factor of the flexural, membrane and shear mode of the structure.

	h (mm)	ρ (kg.m^{-3})	E (GPa)	ν (-)	η (-)
Glass skins	4	2300	62	0.24	0
PVB	0.75	1000	see [9]	0.49	see [9]

Table 4
Characteristics of the automotive glass laminates used by Shorter.

Figure 8 compares the results of Shorter with the ones of the present model using the space domain (Eq. (19)) and energetic (Eq. (25)) definitions. We can see that, with the same definition of the loss factor (energetic), both models give similar results for all three wave types. Some differences appear with the space domain definition concerning the flexural mode (a) in low frequencies. As the damping of the PVB is extremely high ($> 50\%$) in this frequency band, these differences could come from the assumptions of both definitions for high damped structures.

3.6 Comparison with Ghinet: case of an orthotropic multilayered plate

A last validation of the structural loss factor concerns a comparison with the Discrete Laminate Model (DLM) of Ghinet et al. [8] for an orthotropic multilayer. In their model, each layer is described with a displacement field governed by the Reissner-Mindlin theory. In the special case of symmetric sandwich structures, a

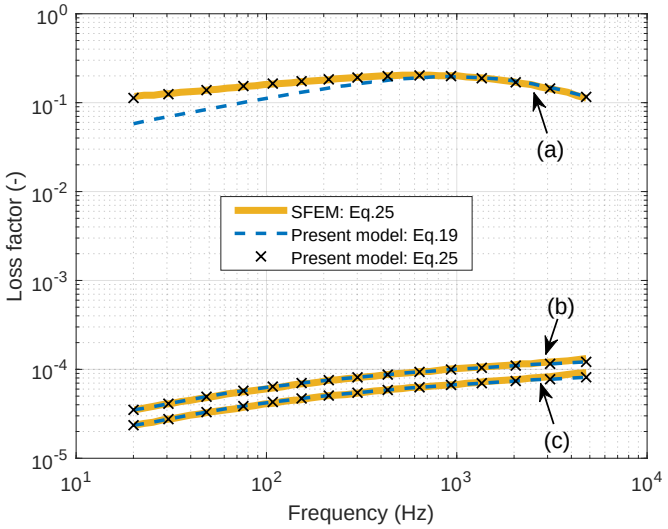

Fig. 8. Structural loss factor η of an automotive glass laminate for three wave types : flexural (a), membrane (b) and shear (c). Solid yellow curves: Eq. (25) with SFEM , black cross: Eq. (25) with the present model, blue dashed curve: Eq. (19) with the present model.

dilatational motion is added along the thickness of the core to describe the symmetrical mode. From the DLM method, Ghinet et al. estimate the loss factor with the energetic approach presented in section 3.3 (Eq. 25). The orthotropic laminates create an angular dependency of the loss factor. To illustrate this, he studied a viscoelastic sandwich with orthotropic skins (see Table 5 for the characteristics).

Skins	Core
h = 1.52 mm	h = 0.127 mm
ρ = 1600 kg.m^{-3}	ρ = 970 kg.m^{-3}
E_x = 125 GPa; E_y = 12.5 GPa	E = 2.1 MPa
$G_{xy} = G_{yz}$ = 5.9 GPa; G_{xz} = 3 GPa	G = 0.7 MPa
ν_{xy} = 0.4	ν = 0.499
η = 0.01	η = 0.5

Table 5
Material characteristics of the composite sandwich plate used by Ghinet et al. [8].

In Figure 9, the structural loss factor η as obtained with the present model (Eq. 19 and Eq. 25) is compared with Ghinet's results for three propagation angles (0°, 45°, 90°) and an average from 0° to 90°. From these results, we can observe that the orthotropy of the structure modifies the value and the position of the maximum of damping as function of the angle. The present model, using the energetic approach (Eq. 25), provides similar results as the ones of Ghinet except for θ =90°. This difference can come from the assumption of constant transverse displacement in our model. We can observe other differences between the results of Eq. 19 and Eq. 25, which can also come from the assumption of the different definitions for

high damped structures.

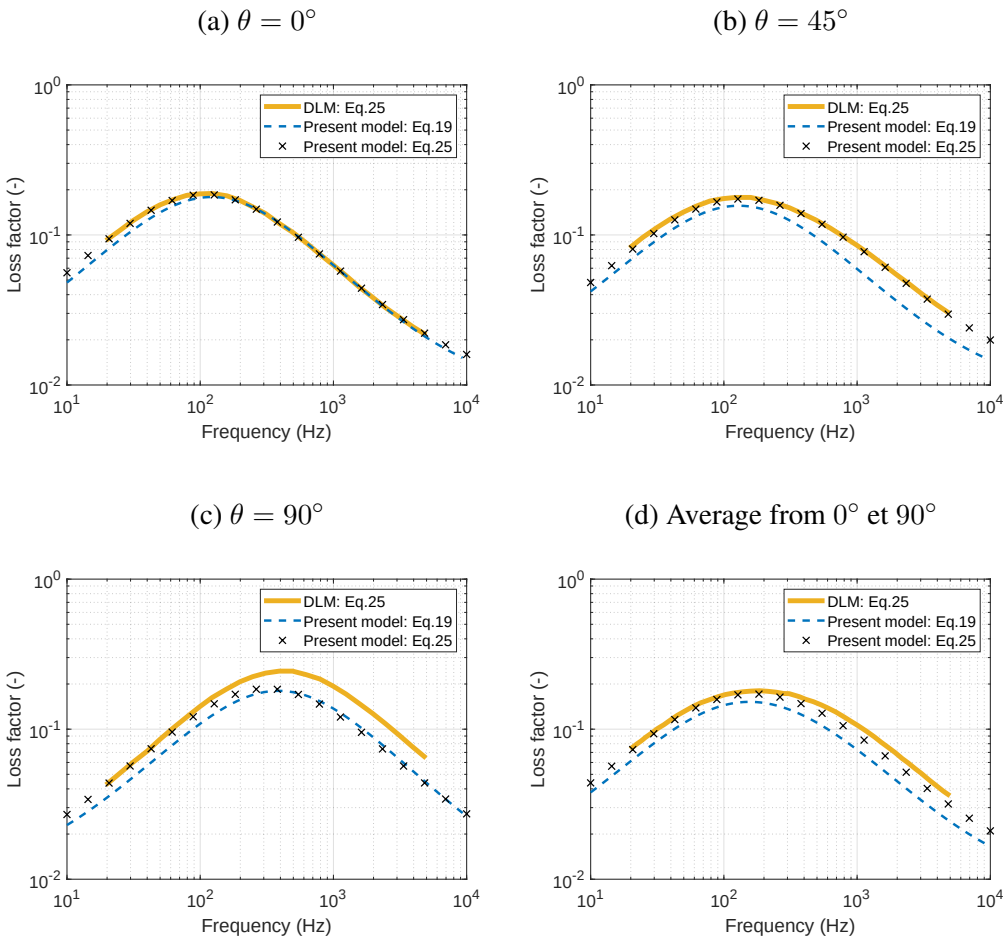

Fig. 9. Structural loss factor of a sandwich composite plate (Graphite-Epoxy skins and viscoelastic core) for three propagation angles θ (0°,45°and 90°) and an average from 0° to 90°. Solid yellow curves: Eq. (25) with the DLM , black cross: Eq. (25) with the present model, blue dashed curve: Eq. (19) with the present model.

4 Experimental estimations of the structural loss factor: validation of the definitions

To validate the different approaches for the estimation of the loss factor, given in Section 3, this section presents measurements of the structural loss factor using the space domain and equivalent definitions for two constrained-layer damping sandwich plates. Analytical results will be presented as well.

4.1 Three-layer plates

The sandwich plates under study are constituted of three homogeneous layers: two metal face sheets and a polymer core. Two sets of hybrid composites are studied: symmetrical steel/polymer/steel (called SPS) and nonsymmetrical steel/polymer/aluminium (called SPA) rectangular plates of overall dimensions of 300×400 mm^2. Layer thicknesses and material properties of the individual layers are listed in Table 6. The thicknesses correspond to average values determined using optical microscope images of the two plates' cross sections. The Young's modulus and loss factor of the polymer layer are estimated thanks to the extrapolations of DMA (Dynamic Mechanical Analysis) measurements performed on sheets of the polymer layer alone [14]. The density is determined by measuring and weighting large specimens.

SPS plate	layer 1 (steel)	layer 2 (polymer)	layer 3 (steel)
Thickness h [m]	0.18×10^{-3}	0.69×10^{-3}	0.18×10^{-3}
Young's modulus E [GPa]	210	0.35	210
Density ρ [kg.m^{-3}]	7800	580	7800
Poisson's ratio ν [-]	0.33	0.33	0.33
Loss factor η [-]	0.001	0.047	0.001
SPA plate	layer 1 (steel)	layer 2 (polymer)	layer 3 (aluminum)
Thickness h [m]	0.3×10^{-3}	0.69×10^{-3}	0.13×10^{-3}
Young's modulus E [GPa]	210	0.35	69
Density ρ [kg.m^{-3}]	7800	580	2700
Poisson's ratio ν [-]	0.33	0.33	0.33
Loss factor η [-]	0.001	0.04	0.001

Table 6
Dimensions and material properties of the individual layers for the two constrained-layer damping sandwich plates chosen for experimental damping characterisation.

4.2 Assessment procedures (theories and experimental setups)

Figure 10 sums up the experimentally identified loss factors together with analytical predictions for both plates. Before discussing the results of these wide frequency bands damping characterisations, we briefly present the experimental protocols and assessment procedures below.

Modal approaches.

a) Modal analysis (△). To begin, a modal analysis of the plate is performed in order to estimate the first modal frequencies and loss factors. A pseudo-impulse force is applied by means of a small impact hammer (P.C.B. Piezotronics 086E80) on a rectangular mesh of 9×11 points spanning the whole 300×400 mm^2 surface of the plate. The mesh is regularly spaced, resulting in spacings between two consecutive points of 37.5 mm along the width x and of 40 mm along the length y. Boundary conditions are kept as close as possible to free-free, by suspending the plate from one of its corner (with rubber bands passing through a tiny hole). The acceleration is measured with a lightweight accelerometer (P.C.B. Piezotronics M353B18) fixed on another corner of the plate. A multi-degree-of-freedom curve fitting method (Rational Fraction Polynomial-Z) is used to estimate modal frequencies and loss factors. For this "low frequency" experimental methodology, modal loss factors have been estimated up to 1 kHz.

b) High resolution modal analysis (ESPRIT methodology) (•). In order to identify the loss factors of the multilayer plate at higher frequencies, a second approach is used. It consists on a high-resolution modal analysis technique [13] based on ESPRIT algorithm [37]. This high-resolution method assumes that the signal $s(t)$ is a sum of complex exponentials $x(t)$ (the modal signal to be determined) and white noise $\beta(t)$. For exponentially damped sinusoids (the signal model considered here), the rotational invariance property of the signal subspace (or *modal* subspace) is used to estimate the modal parameters (see Roy et al. [37] for mathematical developments). Modal frequencies and modal damping factors are derived from the complex poles (eigenvalues of the *spectral matrix* [13]). The experimental protocol is similar to the previous item. The time signal $s(t)$ analysed with ESPRIT algorithm corresponds to an excitation made in the vicinity of the accelerometer near one of the corner of the plate. Modal loss factors have been estimated up to 3 kHz.

Energetic approach.

Time decay rate estimation (□). Impulse responses used for ESPRIT are also processed following a time decay rate estimation method. Signals are firstly filtered through third octave band filters, then the decay rate of the squared envelope is estimated in dB/s using a linear regression. The loss factor for each frequency band is then assessed using the following relation (see [16]):

$$\eta = \frac{\mathrm{DR}}{27.3 f_c}, \tag{26}$$

where DR is the estimated decay rate and f_c the central frequency of the third octave band. Using this third experimental methodology, loss factors have been estimated up to 8 kHz.

Space domain approach.

Displacement field analysis (×) and (×). An experimental procedure, similar to the one presented in section 2.5, has been conducted on the SPS and SPA plates. In these measurements, the position of the source was outside of the measured area. In order to identify the complex material parameters of the structure, the inverse method CFAT [19] has been applied on the measured displacement fields using the filtering procedure of FAT [38] to attenuate noise sensibility on the results. As stated in the introduction, CFAT describes the structure with a Love-Kirchhoff's thin plate and estimates its equation of motion with a finite difference scheme. The complex rigidity and thus the complex flexural wavenumber of the plates have been estimated with this method up to 20 kHz. The structural loss factor has been identified from the estimated complex wavenumber using the equivalent (Eq. (20)) and space domain definition (Eq. (19))

For more details on the assessment procedures presented in this section the reader may refer to Ege et al. [14]. Note that for impulse hammer measurements of the SPA plate, no experimental mesh has been investigated for reason of time-efficiency; the measurement has been done just at one corner of the plate with a relative low sampling frequency, giving results up to 3 kHz with the ESPRIT method only.

4.3 Experimental and analytical comparisons. Discussion

Figure 10 compares the loss factors η_{eq} and η experimentally estimated by the CFAT method and analytically predicted by our model with the results of the modal methods (modal analysis and ESPRIT) and energetic approach (reverberation time). Concerning the loss factor identified by the CFAT method using Eq. (19), the ratio C_{g}/C_{ϕ} is calculated from the analytical wavenumber given by our model. Another strategy giving similar results would be to use a fitting polynomial curve on the experimental wavenumber results.

We can see that the predictions of our model consistently follow the estimations of CFAT for both plates. The results of the modal (blue triangles and dots) and energetic (blue squares) methods follow particularly well the loss factor predicted by the model (blue curves) and estimated by CFAT (blue crosses) using the space domain definition with overlapping estimations in a large frequency domain, demonstrating the validity of the approach developed in this paper. These observations are also in agreement with the fact that the equivalent spatial definition (Eq. (20)) overestimates the loss factor when the behaviour of the structure is highly modified with the frequency band considered (for instance: shearing effects on the flexural motion). Note that the discrepancies in the low freq (for the first modes) could have for origin the hanging system or accelerometer cable, leading to an overestimation of the loss factor.

(a) SPS plate

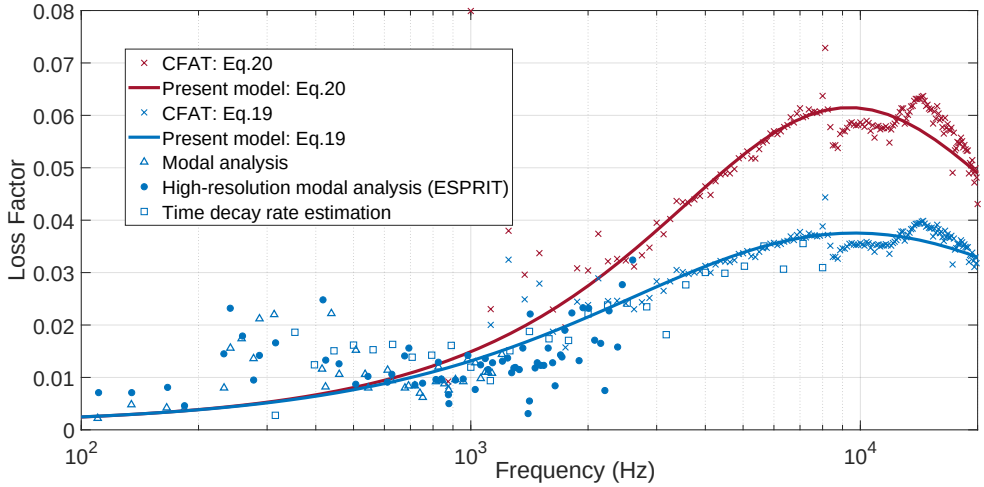

(b) SPA plate

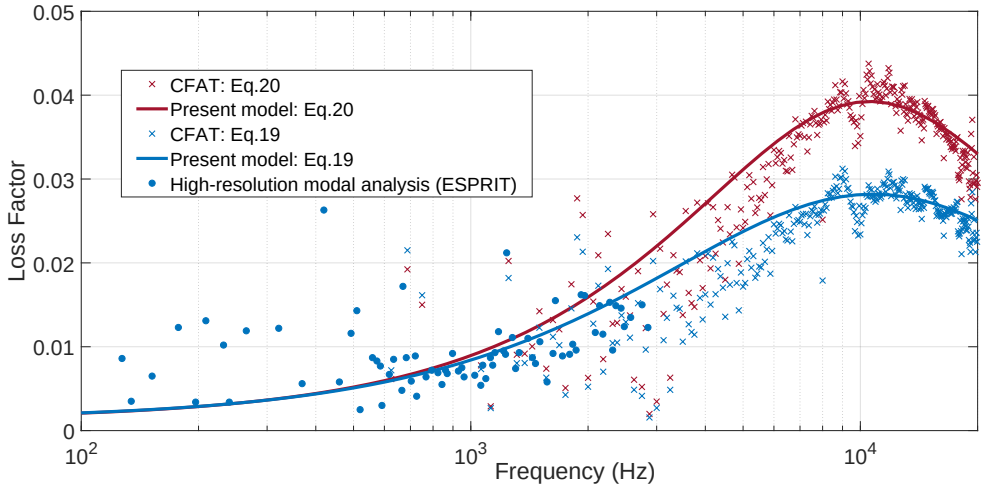

Fig. 10. Structural loss factor of the SPS (a) and SPA (b) sandwich plates (characteristics in Table 6). See the legend of the figures for the line types in the graphs and section 4.2 for the experimental procedures.

Finally, these interesting experimental results, rarely addressed in literature, give a new perspective on damping identification for complex structures. A direct measurement of the complex wavenumber may be sufficient to obtain, using the space domain definition of the loss factor, similar results as energetic or modal methods. This wavenumber can be entirely estimated with spatial experimental methodologies like CFAT but also the ones based on Green's functions for example.

5 Conclusion

This paper is focused on the modelling and the characterisation of laminated multilayered plates and sandwich structures in terms of stiffness and damping. The developments are based on the analytical model of Guyader and Lesueur [11] which considers bending, membrane and shearing effects in each layer. The first novelty of this article consists in adapting the equivalent methodology of characterisation used by Guyader and Cacciolati [12] for laminated structures. As a first step, the dispersion relation of the system is setting up from the work of Woodcock [25] using a symbolic computation given as a supplementary material in the form of a Matlab script. As a second step, the equivalent characteristics of the laminated structure are identified using a thin plate theory defined by 5 flexural rigidities. An experimental validation of this adaptation is performed on a laminated composite plate. The predictions of the analytical model give accurate results compared to the measurements in terms of the bending wavenumber and rigidities.

The concept of equivalent plate provides a computationally more efficient way to design numerically the dynamic response of multilayered structures. The present model provides accurate results for vibro-acoustic studies with a fast computation time as compared to numerical or other analytical models. In an industrial context, an interesting application could be to substitute a 3D multi-layered plate in FEM methods by a 2D homogeneous layer defined with dynamic equivalent parameters given by the presented model. This last point can solve FEM issues where laminated plates must be modelled with a thin mesh in the thickness especially in the high frequency domain. Another perspective of this model could be to explore the high frequency domain (above 20 kHz) and compare its results with more complete model (such as Lamb wave) and experimental data (see for example the recent work of Roozen et al. [39] up to 50 kHz). Other types of waves are excited in this frequency domain and still remain difficult to identify. The optimisation of multi-layered structures could be another application of the model, especially with optimized damping properties for given frequency domains as it was presented in section 3.

The equivalent thin plate theory can also be used in the modelling of the structural loss factor. This equivalent definition is valid for thin structures in low frequencies and overestimates the loss factor in high frequencies when the behaviour of the multilayer is dominated by the shearing of the core. On the contrary, the space domain definition describes this effect by considering the ratio of the group and phase velocities. This ratio can be extracted from the (measured or analytically computed) natural wavenumber. For lightly damped structures, this second definition of the loss factor gives similar results as the MSE approach based on the dissipated power of the structure. The second novelty of the paper is an experimental validation of the space domain definition. The structural loss factors of two sandwich plates are identified from the estimations of the CFAT method [19] using this definition. The

results are in good agreement with the loss factors that were analytically predicted by our model and experimentally estimated by modal and energetic methods.

The space domain definition of the loss factor provides a new perspective on damping identification since the definition is not based on Love-Kirchhoff thin plate theory. The loss factor is computed from the natural wavenumber of the structure which can be easily estimated experimentally. The resulting loss factor estimate is valid for thin and for thick plates. An interesting application could be to use this definition and damping identification methodologies on other complex structures like ribbed panels [28], periodic structures / meta-materials [40] or porous materials.

Acknowledgments

This work was performed within the framework of the Labex CeLyA of Université de Lyon, operated by the French National Research Agency (ANR-10-LABX-0060/ ANR-11-IDEX-0007). The last author (N.B. Roozen) was supported by the H2020-MSCA-RISE-2015 project No. 690970 "Papabuild". The authors would like to express their gratitude to Jean-Louis Guyader for fruitful discussions and the company Hexcel for providing us the three composite plates mentioned in this paper. The authors would like to thank also Céline Sandier (engineer at LVA), Youssef Gerges (postdoctoral fellow at LVA), and master's students Pierre Jailin and Nhu Hai Nguyen for their precious help during measurements.

Appendix

A. Expression of the kinetic matrix [I] used in the equations of motion (3)

$$[I] = \begin{bmatrix} I_1 & -I_2 & -I_3 & -I_4 & -I_5 \\ I_2 & I_6 & I_7 & I_8 & I_9 \\ I_3 & I_7 & I_{10} & I_{11} & I_{12} \\ I_4 & I_8 & I_{11} & I_{13} & I_{14} \\ I_5 & I_9 & I_{12} & I_{14} & I_{15} \end{bmatrix},$$

with

$$I_1 = 2\left[\delta_{13} - \delta_1 \frac{\partial^2}{\partial x^2} - \delta_7 \frac{\partial^2}{\partial y^2}\right],$$

$$I_2 = \delta_5 \frac{\partial}{\partial x},$$

$$I_3 = \delta_4 \frac{\partial}{\partial x} + \delta_{16} \frac{\partial}{\partial y},$$

$$I_4 = \delta_{11} \frac{\partial}{\partial y},$$

$$I_5 = \delta_{15} \frac{\partial}{\partial x} + \delta_{10} \frac{\partial}{\partial y},$$

$$I_6 = 2\delta_3,$$

$$I_7 = \delta_6,$$

$$I_8 = 0,$$

$$I_9 = \delta_{18},$$

$$I_{10} = 2\delta_2,$$

$$I_{11} = \delta_{17},$$

$$I_{12} = \delta_{14},$$

$$I_{13} = 2\delta_9,$$

$$I_{14} = \delta_{12},$$

$$I_{15} = 2\delta_8.$$

B. Expression of the deformation matrix [J] used in the equations of motion (3)

$$[J] = \begin{bmatrix} J_1 & -J_2 & -J_3 & -J_4 & -J_5 \\ J_2 & J_6 & J_7 & J_8 & J_9 \\ J_3 & J_7 & J_{10} & J_{11} & J_{12} \\ J_4 & J_8 & J_{11} & J_{13} & J_{14} \\ J_5 & J_9 & J_{12} & J_{14} & J_{15} \end{bmatrix},$$

with

$$J_1 = 2\left[\lambda_1\frac{\partial^4}{\partial x^4} + (\lambda_{13}+\lambda_{22})\frac{\partial^4}{\partial x^2\partial y^2} + \lambda_7\frac{\partial^4}{\partial y^4} + \lambda_{39}\frac{\partial^4}{\partial x^3\partial y} + \lambda_{54}\frac{\partial^4}{\partial x\partial y^3}\right],$$

$$J_2 = -\left[\lambda_5\frac{\partial^3}{\partial x^3} + (\lambda_{19}+\lambda_{29})\frac{\partial^3}{\partial x\partial y^2} + (\lambda_{41}+\lambda_{45})\frac{\partial^3}{\partial x^2\partial y} + \lambda_{56}\frac{\partial^3}{\partial y^3}\right],$$

$$J_3 = -\left[\lambda_4\frac{\partial^3}{\partial x^3} + (\lambda_{16}+\lambda_{27})\frac{\partial^3}{\partial x\partial y^2} + (\lambda_{40}+\lambda_{42})\frac{\partial^3}{\partial x^2\partial y} + \lambda_{55}\frac{\partial^3}{\partial y^3}\right],$$

$$J_4 = -\left[\lambda_{49}\frac{\partial^3}{\partial x^3} + (\lambda_{60}+\lambda_{64})\frac{\partial^3}{\partial x\partial y^2} + (\lambda_{15}+\lambda_{30})\frac{\partial^3}{\partial x^2\partial y} + \lambda_{11}\frac{\partial^3}{\partial y^3}\right],$$

$$J_5 = -\left[\lambda_{48}\frac{\partial^3}{\partial x^3} + (\lambda_{57}+\lambda_{63})\frac{\partial^3}{\partial x\partial y^2} + (\lambda_{14}+\lambda_{28})\frac{\partial^3}{\partial x^2\partial y} + \lambda_{10}\frac{\partial^3}{\partial y^3}\right],$$

$$J_6 = -2\left[\lambda_3\frac{\partial^2}{\partial x^2} + \lambda_{25}\frac{\partial^2}{\partial y^2} + \lambda_{47}\frac{\partial^2}{\partial x\partial y}\right],$$

$$J_7 = -\left[\lambda_6\frac{\partial^2}{\partial x^2} + \lambda_{32}\frac{\partial^2}{\partial y^2} + (\lambda_{44}+\lambda_{46})\frac{\partial^2}{\partial x\partial y}\right],$$

$$J_8 = -\left[\lambda_{53}\frac{\partial^2}{\partial x^2} + \lambda_{62}\frac{\partial^2}{\partial y^2} + (\lambda_{21}+\lambda_{36})\frac{\partial^2}{\partial x\partial y}\right],$$

$$J_9 = -\left[\lambda_{52}\frac{\partial^2}{\partial x^2} + \lambda_{59}\frac{\partial^2}{\partial y^2} + (\lambda_{20}+\lambda_{34})\frac{\partial^2}{\partial x\partial y}\right],$$

$$J_{10} = -2\left[\lambda_2\frac{\partial^2}{\partial x^2} + \lambda_{23}\frac{\partial^2}{\partial y^2} + \lambda_{43}\frac{\partial^2}{\partial x\partial y} - \lambda_{37}\right],$$

$$J_{11} = -\left[\lambda_{51}\frac{\partial^2}{\partial x^2} + \lambda_{61}\frac{\partial^2}{\partial y^2} + (\lambda_{18}+\lambda_{33})\frac{\partial^2}{\partial x\partial y}\right],$$

$$J_{12} = -\left[\lambda_{50}\frac{\partial^2}{\partial x^2} + \lambda_{58}\frac{\partial^2}{\partial y^2} + (\lambda_{17}+\lambda_{31})\frac{\partial^2}{\partial x\partial y} - \lambda_{69}\right],$$

$$J_{13} = -2\left[\lambda_{26}\frac{\partial^2}{\partial x^2} + \lambda_9\frac{\partial^2}{\partial y^2} + \lambda_{68}\frac{\partial^2}{\partial x\partial y}\right],$$

$$J_{14} = -\left[\lambda_{35}\frac{\partial^2}{\partial x^2} + \lambda_{12}\frac{\partial^2}{\partial y^2} + (\lambda_{66}+\lambda_{67})\frac{\partial^2}{\partial x\partial y}\right],$$

$$J_{15} = -\left[\lambda_{24}\frac{\partial^2}{\partial x^2} + \lambda_8\frac{\partial^2}{\partial y^2} + \lambda_{65}\frac{\partial^2}{\partial x\partial y} - \lambda_{38}\right].$$

C. Expression of the coefficients l_i and d_i used in the stiffness matrix $[\mathcal{K}]$ and mass matrix $[\mathcal{M}]$ in Eq. (5)

$$l_1 = 2(\lambda_1 c^4 + \lambda_{39}c^3 s + (\lambda_{13}+\lambda_{22})c^2 s^2 + \lambda_{54}cs^3 + \lambda_7 s^4),$$

$$l_2 = \lambda_5 c^3 + (\lambda_{41}+\lambda_{45})c^2 s + (\lambda_{19}+\lambda_{29})cs^2 + \lambda_{56}s^3,$$

$$l_3 = \lambda_4 c^3 + (\lambda_{16} + \lambda_{27}) cs^2 + (\lambda_{40} + \lambda_{42}) c^2 s + \lambda_{55} s^3,$$

$$l_4 = \lambda_{49} c^3 + (\lambda_{60} + \lambda_{64}) cs^2 + (\lambda_{15} + \lambda_{30}) c^2 s + \lambda_{11} s^3,$$

$$l_5 = \lambda_{48} c^3 + (\lambda_{57} + \lambda_{63}) cs^2 + (\lambda_{14} + \lambda_{28}) c^2 s + \lambda_{10} s^3,$$

$$l_6 = 2(\lambda_3 c^2 + \lambda_{25} s^2 + \lambda_{47} cs),$$

$$l_7 = \lambda_6 c^2 + \lambda_{32} s^2 + (\lambda_{44} + \lambda_{46}) cs,$$

$$l_8 = \lambda_{53} c^2 + \lambda_{62} s^2 + (\lambda_{21} + \lambda_{36}) cs,$$

$$l_9 = \lambda_{52} c^2 + \lambda_{59} s^2 + (\lambda_{20} + \lambda_{34}) cs,$$

$$l_{10} = 2(\lambda_2 c^2 + \lambda_{23} s^2 + \lambda_{43} cs),$$

$$l_{11} = \lambda_{51} c^2 + \lambda_{61} s^2 + (\lambda_{18} + \lambda_{33}) cs,$$

$$l_{12} = \lambda_{50} c^2 + \lambda_{58} s^2 + (\lambda_{17} + \lambda_{31}) cs,$$

$$l_{13} = 2(\lambda_{26} c^2 + \lambda_9 s^2 + \lambda_{68} cs),$$

$$l_{14} = \lambda_{35} c^2 + \lambda_{12} s^2 + (\lambda_{66} + \lambda_{67}) cs,$$

$$l_{15} = 2(\lambda_{24} c^2 + \lambda_8 s^2 + \lambda_{65} cs),$$

$$l_{37} = 2\lambda_{37},$$

$$l_{38} = 2\lambda_{38},$$

$$l_{69} = \lambda_{69},$$

$$d_1 = 2\omega^2 \left(\delta_1 c^2 + \delta_7 s^2\right),$$

$$d_2 = \delta_5 c,$$

$$d_3 = \left(\delta_4 c + \delta_{16} s\right),$$

$$d_4 = \delta_{11} s,$$

$$d_5 = \left(\delta_{15} c + \delta_{10} s\right),$$

$$d_6 = 2\delta_3,$$

$$d_7 = \delta_6,$$

$$d_8 = 2\delta_{13},$$

$$d_9 = \delta_{18},$$

$$d_{10} = 2\delta_2,$$

$$d_{11} = \delta_{17},$$

$$d_{12} = \delta_{14},$$

$$d_{13} = 2\delta_9,$$

$$d_{14} = \delta_{12},$$

$$d_{15} = 2\delta_8,$$

with : $c = \cos(\theta)$ and $s = \sin(\theta)$.

References

[1] E. Carrera, An assessment of mixed and classical theories on global and local response of multilayered orthotropic plates, Composite Structures 50 (2) (2000) 183 – 198.
URL http://www.sciencedirect.com/science/article/pii/S0263822300000994

[2] D. Ross, E. Kerwin, E. E. Ungar, Damping of plate flexural vibrations by means of viscoelastic laminae, Structural Damping 3 (1959) 44–87.

[3] E. M. Kerwin, Damping of flexural waves by a constrained viscoelastic layer, The Journal of the Acoustical Society of America 31 (7) (1959) 952–962.
URL https://doi.org/10.1121/1.1907821

[4] E. E. Ungar, E. M. Kerwin, Loss factors of viscoelastic systems in terms of energy concepts, The Journal of the Acoustical Society of America 34 (7) (1962) 954–957.
URL https://doi.org/10.1121/1.1918227

[5] E. Nilsson, A. Nilsson, Prediction and measurement of some dynamic properties of sandwich structures with honeycomb and foam cores, Journal of Sound and Vibration 251 (3) (2002) 409 – 430.
URL http://www.sciencedirect.com/science/article/pii/S0022460X01940076

[6] D. Backström, A. Nilsson, Modelling the vibration of sandwich beams using frequency-dependent parameters, Journal of Sound and Vibration 300 (3) (2007) 589 – 611.

URL http://www.sciencedirect.com/science/article/pii/S0022460X06007115

[7] A. Nilsson, S. Baro, E. A. Piana, Vibro-acoustic properties of sandwich structures, Applied Acoustics 139 (2018) 259 – 266.
URL http://www.sciencedirect.com/science/article/pii/S0003682X17307909

[8] S. Ghinet, N. Atalla, Modeling thick composite laminate and sandwich structures with linear viscoelastic damping, Computers and Structures 89 (15) (2011) 1547 – 1561.
URL http://www.sciencedirect.com/science/article/pii/S0045794911001295

[9] P. J. Shorter, Wave propagation and damping in linear viscoelastic laminates, The Journal of the Acoustical Society of America 115 (5) (2004) 1917–1925.
URL https://doi.org/10.1121/1.1689342

[10] E. Manconi, B. R. Mace, Estimation of the loss factor of viscoelastic laminated panels from finite element analysis, Journal of Sound and Vibration 329 (19) (2010) 3928 – 3939.
URL http://www.sciencedirect.com/science/article/pii/S0022460X1000266X

[11] J. L. Guyader, C. Lesueur, Acoustic transmission through orthotropic multilayered plates, part 1: Plate vibration modes, Journal of Sound and Vibration 58 (1) (1978) 51 – 68.
URL http://www.sciencedirect.com/science/article/pii/S0022460X78800601

[12] J. L. Guyader, C. Cacciolati, Viscoelastic properties of single layer plate material equivalent to multi-layer composites plate, Internoise (2007) 1558–1567.

[13] K. Ege, X. Boutillon, B. David, High-resolution modal analysis, Journal of Sound and Vibration 325 (4) (2009) 852 – 869.
URL http://www.sciencedirect.com/science/article/pii/S0022460X09003447

[14] K. Ege, N. B. Roozen, Q. Leclère, R. G. Rinaldi, Assessment of the apparent bending stiffness and damping of multilayer plates; modelling and experiment, Journal of Sound and Vibration 426 (2018) 129 – 149.
URL http://www.sciencedirect.com/science/article/pii/S0022460X18302384

[15] J. Berthaut, M. Ichchou, L. Jezequel, K-space identification of apparent structural behaviour, Journal of Sound and Vibration 280 (3) (2005) 1125 – 1131.
URL http://www.sciencedirect.com/science/article/pii/S0022460X04002925

[16] R. Cherif, J.-D. Chazot, N. Atalla, Damping loss factor estimation of two-dimensional orthotropic structures from a displacement field measurement, Journal of Sound and Vibration 356 (2015) 61 – 71.

URL http://www.sciencedirect.com/science/article/pii/S0022460X1500543X

[17] J. Cuenca, F. Gautier, L. Simon, The image source method for calculating the vibrations of simply supported convex polygonal plates, Journal of Sound and Vibration 322 (4) (2009) 1048 – 1069.
URL http://www.sciencedirect.com/science/article/pii/S0022460X08009334

[18] N. B. Roozen, Q. Leclère, K. Ege, Y. Gerges, Estimation of plate material properties by means of a complex wavenumber fit using Hankel's functions and the image source method, Journal of Sound and Vibration 390 (2017) 257 – 271.
URL http://www.sciencedirect.com/science/article/pii/S0022460X16307118

[19] Q. Leclère, F. Ablitzer, C. Pézerat, Practical implementation of the corrected force analysis technique to identify the structural parameter and load distributions, Journal of Sound and Vibration 351 (2015) 106 – 118.
URL http://www.sciencedirect.com/science/article/pii/S0022460X15003570

[20] F. Marchetti, K. Ege, Q. Leclère, Localisation and identification of sources on laminated structures: extension of CFAT method, in: Noise and vibration: Emerging methods - NOVEM 2018, Ibiza, Spain, 2018, p. 171981.
URL https://hal.archives-ouvertes.fr/hal-01790339

[21] A. Berry, O. Robin, F. Pierron, Identification of dynamic loading on a bending plate using the virtual fields method, Journal of Sound and Vibration 333 (26) (2014) 7151 – 7164.
URL http://www.sciencedirect.com/science/article/pii/S0022460X1400710X

[22] A. Berry, O. Robin, P. O'Donoughue, Identifying dynamic constitutive parameters of bending plates using the virtual fields method, in: M. Sutton, P. L. Reu (Eds.), International Digital Imaging Correlation Society, Springer International Publishing, Cham, 2017, pp. 5–8.

[23] P. Margerit, A. Lebée, J.-F. Caron, X. Boutillon, High resolution wavenumber analysis (hrwa) for the mechanical characterisation of viscoelastic beams, Journal of Sound and Vibration 433 (2018) 198 – 211.
URL http://www.sciencedirect.com/science/article/pii/S0022460X18304309

[24] P. Margerit, A. Lebée, J.-F. Caron, K. Ege, X. Boutillon, The high-resolution wavevector analysis for the characterization of the dynamic response of composite plates, Journal of Sound and Vibration 458 (2019) 177 – 196.
URL http://www.sciencedirect.com/science/article/pii/S0022460X19303657

[25] R. L. Woodcock, Free vibration of advanced anisotropic multilayered composites with arbitrary boundary conditions, Journal of Sound and Vibration 312 (4) (2008) 769 –

788.
URL http://www.sciencedirect.com/science/article/pii/S0022460X07009091

[26] I. A. Viktorov, Rayleigh and Lamb Waves: Physical Theory and Applications. Transl. from Russian. With a Foreword by Warren P. Mason, Plenum press, 1967.

[27] A. Loredo, A. Castel, A multilayer anisotropic plate model with warping functions for the study of vibrations reformulated from Woodcock's work, Journal of Sound and Vibration 332 (1) (2013) 102 – 125.
URL http://www.sciencedirect.com/science/article/pii/S0022460X12005597

[28] G. Tufano, F. Errico, O. Robin, C. Droz, M. Ichchou, B. Pluymers, W. Desmet, N. Atalla, K-space analysis of complex large-scale meta-structures using the inhomogeneous wave correlation method, Mechanical Systems and Signal Processing 135 (2020) 106407.
URL http://www.sciencedirect.com/science/article/pii/S0888327019306284

[29] R. Lyon, R. DeJong, Theory and application of Statistical Energy Analysis (2nd edition), Butterworth Heinemann, 1995.

[30] J. Berthaut, Contribution à l'identification large bande des structures anisotropes : Application aux tables d'harmonie des pianos, Ph.D. thesis, Ecole Centrale de Lyon (6 2004).

[31] M. Rak, M. Ichchou, J. Holnicki-Szulc, Identification of structural loss factor from spatially distributed measurements on beams with viscoelastic layer, Journal of Sound and Vibration 310 (4) (2008) 801 – 811.
URL http://www.sciencedirect.com/science/article/pii/S0022460X07009212

[32] J. McDaniel, P. Dupont, L. Salvino, A wave approach to estimating frequency-dependent damping under transient loading, Journal of Sound and Vibration 231 (2) (2000) 433 – 449.
URL http://www.sciencedirect.com/science/article/pii/S0022460X99927232

[33] J. Woodhouse, Linear damping models for structural vibration, Journal of Sound and Vibration 215 (3) (1998) 547 – 569.
URL http://www.sciencedirect.com/science/article/pii/S0022460X98917096

[34] P. Millithaler, J.-B. Dupont, M. Ouisse, E. Sadoulet-Reboul, N. Bouhaddi, Viscoelastic property tuning for reducing noise radiated by switched-reluctance machines, Journal of Sound and Vibration 407 (2017) 191 – 208.
URL http://www.sciencedirect.com/science/article/pii/S0022460X17305242

[35] K. Ege, V. Henry, Q. Leclère, R. G. Rinaldi, C. Sandier, Vibrational behavior of multi-layer plates in broad-band frequency range: comparisons between experimental and

theoretical estimations, in: InterNoise 2015, San Francisco, United States, 2015, p. 218.
URL https://hal.archives-ouvertes.fr/hal-01215310

[36] P. Butaud, E. Foltête, M. Ouisse, Sandwich structures with tunable damping properties: On the use of shape memory polymer as viscoelastic core, Composite Structures 153 (2016) 401 – 408.
URL http://www.sciencedirect.com/science/article/pii/S0263822316309783

[37] R. Roy, T. Kailath, Esprit-estimation of signal parameters via rotational invariance techniques, IEEE Transactions on Acoustics, Speech, and Signal Processing 37 (7) (1989) 984–995.
URL https://ieeexplore.ieee.org/document/32276

[38] F. Ablitzer, C. Pézerat, J. Génevaux, J. Bégué, Identification of stiffness and damping properties of plates by using the local equation of motion, Journal of Sound and Vibration 333 (9) (2014) 2454 – 2468.
URL http://www.sciencedirect.com/science/article/pii/S0022460X13010535

[39] N. B. Roozen, L. Labelle, Q. Leclère, K. Ege, S. Alvarado, Non-contact experimental assessment of apparent dynamic stiffness of constrained-layer damping sandwich plates in a broad frequency range using a nd:yag pump laser and a laser doppler vibrometer, Journal of Sound and Vibration 395 (2017) 90 – 101.
URL http://www.sciencedirect.com/science/article/pii/S0022460X17301050

[40] A. Pelat, T. Gallot, F. Gautier, On the control of the first bragg band gap in periodic continuously corrugated beam for flexural vibration, Journal of Sound and Vibration 446 (2019) 249 – 262.

List of Figures

List of Tables